Research Journal of Applied Sciences, Engineering and Technology 6(4): 598-608, 2013
ISSN: 2040-7459; e-ISSN: 2040-7467

Submitted: August 24, 2012 Accepted: September 19, 2012 Published: June 20, 2013

The Interaction of Oscillating-Grid Turbulence with a Sediment Layer

W.H.M. Wan Mohtar and N.M. Zakaria
Department of Civil and Structural Engineering, Faculty of Engineering, National Universiti Kebangsaan, Malaysia, 43600 Bandar Baru Bangi, Selangor, Malaysia

Abstract: This study described a preliminary experimental setup to identify how near-bed turbulence interacts with and moves sediment. The turbulence generated by a vertically oscillating grid was made to interact with a homogeneous horizontal sediment layer. Near-spherical particles were used throughout with two types of sediment at comparable sediment size $d \approx 700$ μm. The interaction characteristics were investigated by employing the PIV technique to measure the velocity field of the displaced sediment grains (within the transverse plane of the bed surface) during the interaction. Measurement of the velocity of the displaced sediment grains was restricted to the $\frac{\theta}{\theta_c} > 1$ case, where $\theta = \frac{\tau_b}{(s-1)gd}$ is the Shields parameter, the subscript c denotes critical i.e. threshold criteria, τ_b is the mean bed shear stress and s is relative density of sediment. During the period of interaction, the sediment grains were primarily displaced by the radial velocities and formed distinctive circular trajectories. Energetic turbulence resuspends the particles above the bed surface, forming the characteristics particle splash.

Keywords: Sediment trajectories turbulence-particle interaction, zero-mean turbulence

INTRODUCTION

Sediment transport is an important phenomenon of great significance impacts in many environmental/ geophysical and industrial contexts, including erosion on agricultural land and contributing as catalyst, carrier and storage agent for major water pollutants. For decades, predicting how fluid transports sediment was based on the models developed in steady turbulent channel flows. The near-bed turbulent fluctuations, which give rise to the hydrodynamic drag and lift forces that induce the sediment motion are correlated with time averaged mean velocity. Hence, most of the prediction of empirical or semi-empirical sediment transport models are the time-averaged bed shear stress τ_b, with effects due to turbulent fluctuations are considered implicitly (Shields, 1936; Lamb *et al*., 2008).

However, in many naturally occurring flows, as noted by previous studies, the simplifications of using mean bed shear stress gives inaccurate prediction of sediment transport (Sumer *et al*., 2003; Wu *et al*., 2008). The intensity of the turbulent fluctuations in the near-bed region can vary significantly with bed position and time due to factors such as external turbulence generated by flow obstacles, local bed geometry or intermittent interaction with coherent vortex structures (McLean *et al*., 1994; Kaftori *et al*., 1995; Nino and Garcia, 1996). In such flow, the near-bed turbulence no longer scales with the mean flow characteristics and the role of turbulent fluctuations should be considered explicitly. Thus, as noted by Schmeeckle *et al*. (1998), predicting sediment motion or bed evolution requires a detailed understanding of the interaction of turbulence with sediment particles.

The experiments described in this study attempt to address this issue and report the turbulence-sediment interaction in the presence of effectively free mean flow, thereby allowing the affect of turbulence to be considered in isolation. Turbulence generated by a vertically oscillating-grid produced an approximation of a zero-mean, quasi-isotropic homogeneous turbulence at distance further away from the grid. At this distance, the root mean square (rms) horizontal velocity u is empirically presented as:

$$u = CfS^{3/2}M^{1/2}\mathcal{Z}^{-1} \quad (1)$$

where C is the empirical constant, f and S is the frequency and stroke of oscillation, respectively, M is the mesh size and $\mathcal{Z}$ is the distance from the grid, where $\mathcal{Z} = 0$ is the grid mid-plane (Hopfinger and Toly, 1976). The validity of Eq. (1) (only) holds at distance further away from the grid, usually at $\mathcal{Z} \geq 2.5$ M (Hopfinger and Toly, 1976; Cheng and Law, 2001). The isotropy and homogeneity characteristics of the turbulence produced has made oscillating-grid

Corresponding Author: W.H.M. Wan Mohtar, Department of Civil and Structural Engineering, Faculty of Engineering, National Universiti Kebangsaan Malaysia, 43600 Bandar Baru Bangi, Selangor, Malaysia, Tel.: +60389216967; Fax: +60389216147

attractive method to investigate geophysical phenomenon such as the incipient sediment motion (Bellinsky *et al*., 2005) and desorption of contaminants from sediment (Valsaraj *et al*., 1997), to name a few.

Preliminary experimental results on the interaction between turbulence (generated by oscillating-grid) and a sediment layer will be discussed. Measurement of the velocity of the displaced sediment grains was restricted to the $d \approx 700$ and two sediment types with comparable sizes. These restrictions preclude using the sediment velocity data for an in-depth parametric analysis. The objective of the study was to provide novel data that could be used to illustrate in detail the impact characteristics of sediment trajectory under the influence of zero-mean turbulence.

EXPERIMENTAL APPARATUS AND SETUP

A sketch of experimental apparatus is shown in Fig. 1. The experiments were performed in an acrylic tank, with cross-sectional dimensions of 35.4 × 35.4 cm^2 and a height of 50 cm. The tank is fixed within a rigid inner steel frame and filled with water to a depth of 40 cm. The oscillating-grid mechanism, consists of a linear bearing was positioned vertically through the central axis of the tank and connected to a rotating spindle. A motor is used to rotate the spindle and thus continuously oscillate the grid. The uniform grid is made from 7×7 array of aluminium square (d_g= 1 cm) bars and length of 35 cm. The uniform mesh size M is 5 cm and gives the grid a solidity of 36 %. The stroke S and oscillation frequency f of the grid were varied by altering the radius of spindle motion on the motor and the rotation rate of the motor, respectively. The grid was positioned so that the bed surface was always at $\mathcal{Z} \approx 2.5M - 2.6M$. For consistency, a stroke of 8 cm was used throughout with frequency varied between 3 to 3.1 Hz, resulting in Reynolds numbers $Re_M = fSM/\upsilon$ (based on the external grid parameters) of approximately 12000.

The sediment types used were ballotini (Particle A) and diakon (Particle B) with comparable sediment sizes of $d \approx 701$ and 750 μm, respectively. These two types of particle were chosen as sediment size $d > 700$ μm was required to resolve the structure of the sediment grains in the images captured. Note that a too energetic

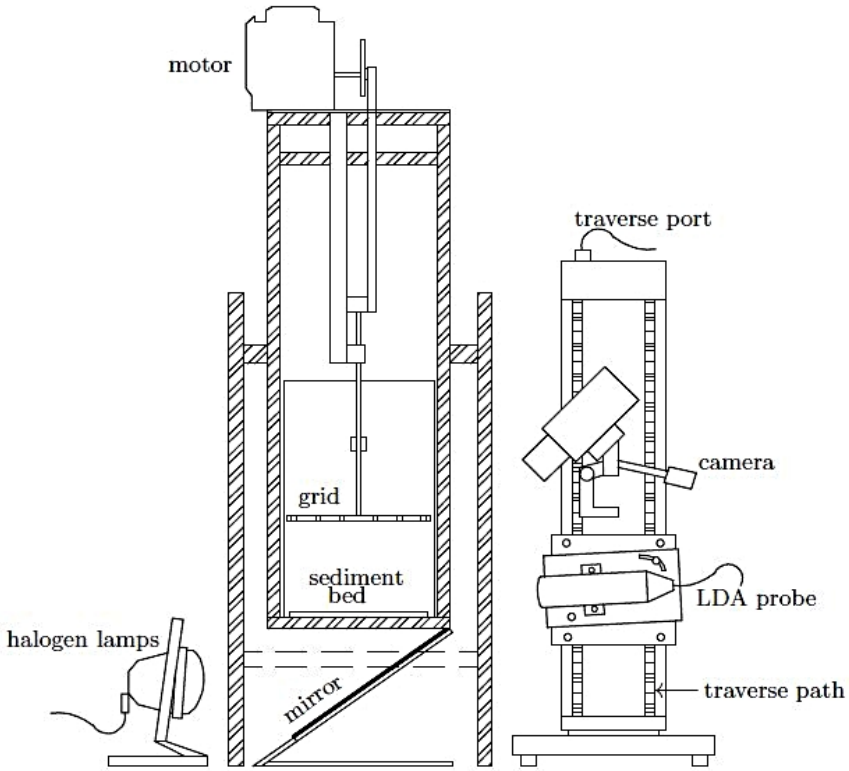

Fig. 1: A side view schematic representation of the experimental setup for the turbulence-sediment interaction experiments. The LDA probe is attached to a plate that can be tilted up to 5°, and is mounted on a traverse system .

Table 1: Summary of experimental parameters

Particle	S	f	θ/θ_c	Re_M (x 10^3)
A	2.50	3.1	4.26	12.6
B	1.18	3	4.76	12.2

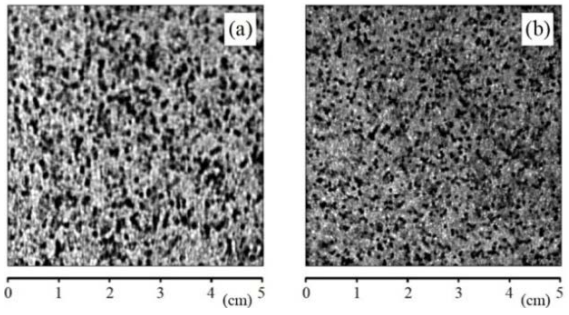

Fig. 2: Images showing two different layers of mixed black and transparent particles of (a) ballotini and (b) diakon. In both images, the mixture ratio is 30% black, 70% transparent and the region shown is an area of 5 x 5 cm^2 on the bed surface

interaction could result in a significant number of sediment grains being resuspended above the impact region, which would obstruct the camera view and affect the sediment velocity measurements (Munro *et al*., 2009). For this reason, particularly for Particle B due to low density, attention was restricted to impacts (of sediment motion and trajectory) which resulted in a minimal level of resuspension. The experimental parameters i.e., the frequency f used, corresponding values of θ/θ_c and Re_M are summarised in Table 1.

The sediment bed is prepared on a fixed tray of 1 cm depth by carefully scraping the bed across the top rim of the tray, which produced a flat packed bed. Once the bed is prepared, the grid-generated turbulence is made to interact with the sediment layer at the specified frequency as described in Table 1. The velocity of the displaced sediment grains were measured using a simple adaptation of standard PIV. In this case, a random pattern structure was established within the bed using black sediment grains added to and mixed thoroughly with, the otherwise transparent sediment. The transparent sediment bed is illuminated by using two high power halogen lamps and the light was directed up into the tank by a mirror located beneath the tank base (Fig. 1). To track the sediment motion, black opaque sediment grains (with ratio 10:1 transparent to black) acted as tracer particles. Images of the two seeded sediment layers produced in this way (prior to impact) are shown in Fig. 2. In each case, the basic properties of the black particles were the same as those corresponding to the transparent sediment. The sediment motion and trajectories are captured by a high speed digital camera which was supported on a tripod and positioned to view down onto the sediment layer. The images were captured using the NanoSense II high speed camera with 1024x1280 pixel resolution at 12 bits per pixel, used in conjunction with a Nikon Zoom-Nikkor 60 mm F2.8- 11 lens. The digital camera was positioned at a distance of 20 cm from the tank and was focused to view vertically down onto the sediment layer surface at an angle of approximately 53.1°. This was the maximum permissible angle to avoid any image distortion caused by the perspex tank. Note that the camera could not be positioned to view vertically down into the tank due to the obstruction of the grid. The camera was positioned to capture as wide as possible region of the sediment bed while still sufficiently resolving the structure of the grains in the bed. As the turbulence interacted with and displaced the near-surface sediments, the motion and trajectories of the tracer grains were captured in the images. Measurements of the particle trajectories were obtained using standard PIV software, using an interrogation window of 15×15 square pixels. To satisfactorily resolve the short time scale associated with each eddy impact, it was necessary for the image sequences to be captured using the high speed camera sampling at 200 and 400 Hz for particle B and A, respectively.

Within the field of view, intermittent sediment motions could occur randomly in the sediment plane. It should be noted that due to the tilted view of the PIV camera, the spatial resolution in the y (transverse) direction is limited. To obtain the physical scale of velocity, the pixel image coordinates were converted to physical coordinates using the linear-mapping procedure. For this, an array of 1 × 1 cm^2 grids was placed on the bottom of the tank and an image was taken. The physical grid was then used to identify orthogonal points that could be used in the mapping procedure. For each set of experiments, the sediment velocity data was obtained during the entire experimental period. The sediment velocity fields were obtained in terms of the right-handed Cartesian coordinates$(x, y, 0)$, defined by the (x, y) axes in the transverse plane of the bed surface at $\xi = 0$ (Fig. 1). The particle velocities denoted by $u_p(x, y, 0)$ and $v_p(x, y, 0)$ for the horizontal and transverse components respectively, were obtained under the same interaction conditions and at corresponding times during the impact.

The fluid velocity measurements (to calculate θ) were obtained using a 2D Laser Doppler Anemometry (LDA) FlowLite optic (Dantec dynamics) operating in the back scatter mode. The LDA probe was placed at distance of approximately 10 cm from the tank and at a height parallel to the sediment bed. In order to (closely)

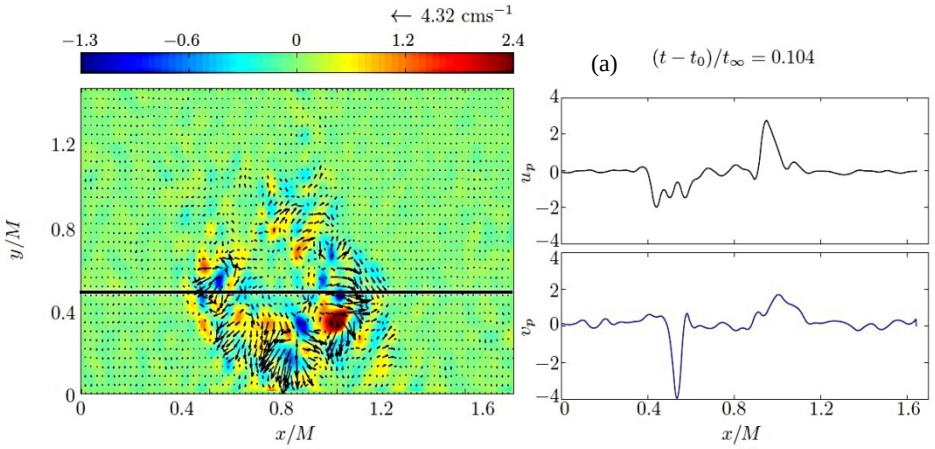
← 4.32 cms^{-1}
−1.3
−0.6
0
1.2
2.4
(a)
$(t-t_0)/t_\infty = 0.104$
y/M
x/M
u_p
v_p

(a)

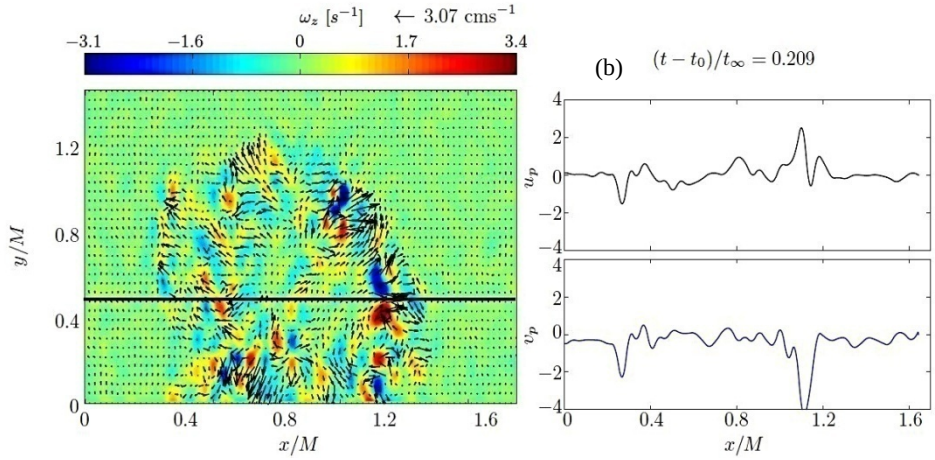
ω_z [s^{-1}]
← 3.07 cms^{-1}
−3.1
−1.6
0
1.7
3.4
(b)
$(t-t_0)/t_\infty = 0.209$
y/M
x/M
u_p
v_p

(b)

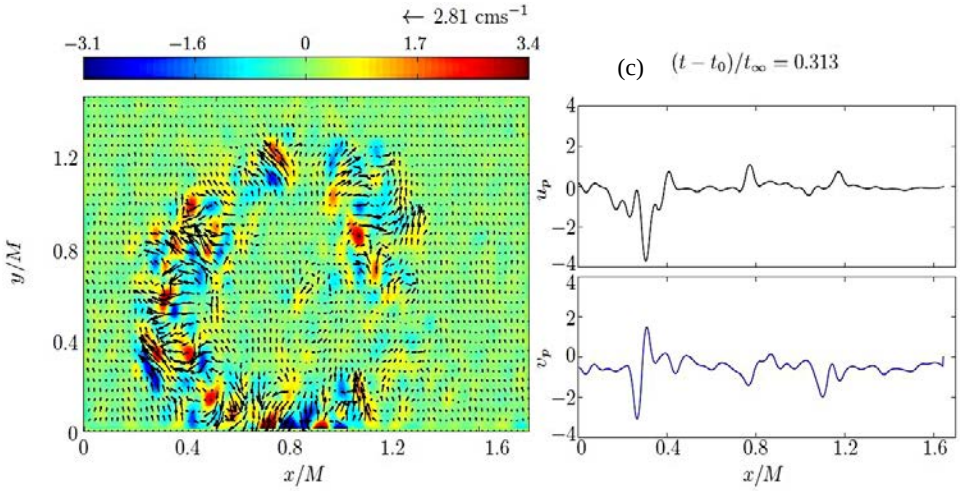
← 2.81 cms^{-1}
−3.1
−1.6
0
1.7
3.4
(c)
$(t-t_0)/t_\infty = 0.313$
y/M
x/M
u_p
v_p

(c)

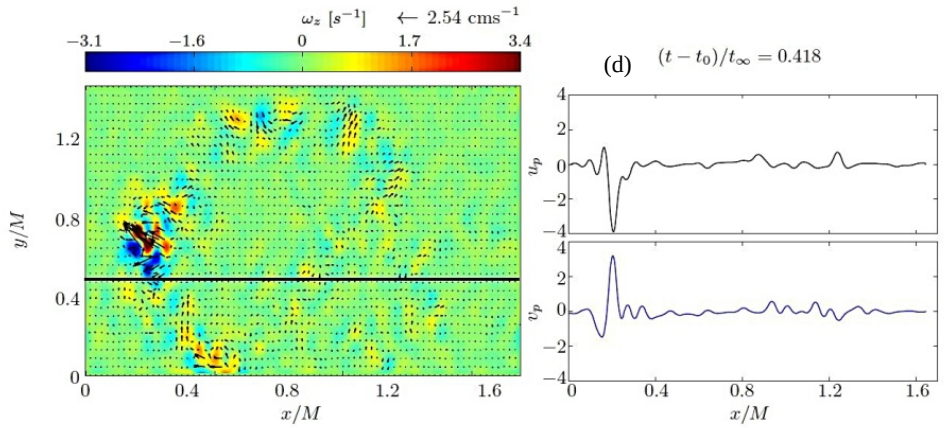

(d)

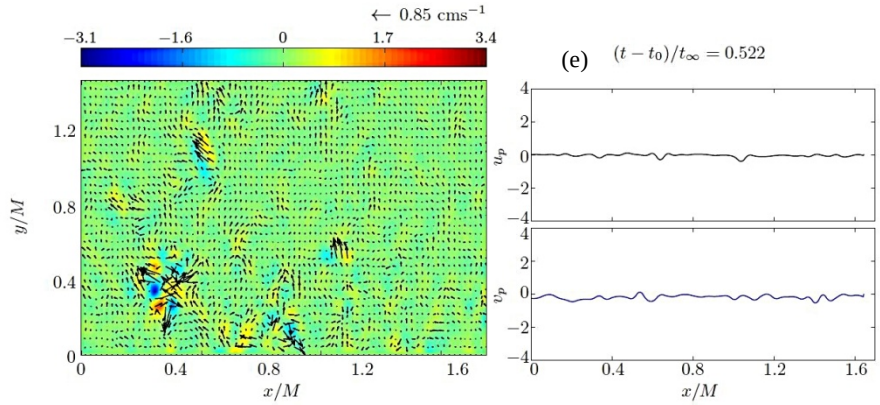

(e)

Fig. 3: Sequences of measured particle velocity fields for Particle A ($d = 701\mu m$) with vorticity $\omega_z = \partial u_p/\partial y - \partial v_p/\partial x$ distributions (shown as left figure) and corresponding horizontal u_p and transverse particle velocity v_p at a fixed point obtained at corresponding dimensionless times with t_∞ = 0.723. The impact shown corresponds to turbulence produced from S = 8 cm, f = 3.1 Hz, θ/θ_c = 4.26 interacting with a sediment layer of particle B. Correspond maximum horizontal particle velocity is shown on the top right corner of left figure. The solid black line in (b) illustrates the corresponding y−point where u_p and v_p were taken

represent the actual fluid velocity acting on the particle, it was imperative for detailed flow measurements to be made at points near to the sediment bed. Therefore, the LDA laser beams were directed into the tank through the side wall so that the beam intersection point (with measuring volume of approximately 650 μm in length and 77 μm in diameter) was positioned at height ξ = 0.5 cm above the bed, corresponding to the point of r.m.s. horizontal velocity amplification. Within this setup, the average sampling rate of the LDA was approximately $10 - 50$ Hz and the measurement was taken at sampling period $T = 90$ s.

As the tap water was used to fill in the tank, the dissolved minerals present in the water were sufficient enough to act as tracer particles. However, to improve the LDA sampling rate, a small volume amount of polyamide particles (ρ_s= 1.03 g/cm^3) with mean diameter of 5 μm were added. The signal response of the LDA was processed by a DANTEC 57N10 Burst Spectrum Analyser (BSA). The BSA software analysed each burst and obtained the velocity measurements from the frequency of the scattered light signal. The detection mode used is `coincident', which enabled simultaneous measurements of both horizontal and vertical velocity components. The (instantaneous)

measured fluid velocities will be denoted by horizontal $\tilde{u}_f(t)$ and vertical $\tilde{w}_f(t)$, respectively. Thus, the Shields parameter θ presented in Table 1 was calculated a:

$$\theta = \frac{u_f^2}{(s-1)gd}, \quad (2)$$

where g is gravity and u_f is the r.m.s. horizontal fluid velocity, which is calculated as:

$$u_f = \left(\overline{u_f'^2}\right)^{1/2} = \sqrt{\frac{1}{N-1}\sum_{n=1}^{N}\left(\tilde{u}_f(t_n) - \bar{u}_f\right)^2} \quad (3)$$

where u_f' and $\bar{u}_f$ are the fluctuating and mean fluid velocities, respectively and $n = 1,2,3,\ldots,N$ and N is the total population of $\tilde{u}_f$.

For sediment interaction close to the critical condition (i.e., $1 \leq \theta/\theta_c < 1.5$), it was noted that only a minimal amount of sediment motion was induced. Hence, to ensure that detectable and/or observable levels of sediment motion occurred, the experiments were performed in the range $\frac{\theta}{\theta_c} \approx 4.3$ and 4.8. The θ_c values for each sediment type were obtained by incrementally increased the oscillation frequency from an initial value of 1 Hz to the point of `critical' frequency at which point incipient grain motion was first observed. The critical Shields parameter θ_c is then calculated using Eq. (2), with oscillation frequency is set at the critical frequency and u_f obtained is the critical r.m.s horizontal fluid velocity.

RESULTS

A qualitative description of typical sediment `splash' induced by the interacting turbulence is presented. The term splash is used here to characterise the typical sediment movement induced by the impingement of an energetic eddy with the sediment bed (Munro *et al*., 2009). Recall that we will present the data of two sediment types: Particle A with θ/θ_c= 4.26 and Particle B with θ/θ_c = 4.76. Note that from Table 1, the level of flow strength at near-bed region is comparable for both sets of data. Throughout the period of capturing images, intermittent energetic sediment movement on the bed surface was observed. However, to describe the sediment's motion, we isolate one energetic interaction for each data set. Upon scrutinizing approximately 10 frames at the initially identified interaction period, the point from which particle movement was visible to the naked eye was taken to be t_0 with the range of the t_0 error circa ± 0.0125 - 0.025 s (≈ 5 frames).

Figure 3a to e and 4a to h illustrate a typical splash event, shown in a transverse plane of particle velocity fields with vortices distributions as background for Particle B (θ/θ_c = 4.26) and Particle H (θ/θ_c= 4.76), respectively. To prevent data saturation, only every the 30th velocity vector has been included in each of the velocity fields shown in Fig. 3 and 4. For each impact, the corresponding horizontal and transverse particle velocities at one fixed point (in the y-direction), denote as $u_p(x)$ and $v_p(x)$ respectively are shown at the right side. The point is usually taken corresponding to the middle of the eddy impingement, shown as thick black line for each case (Fig. 3b). Corresponding dimensionless times $(t - t_0)/t_\infty$ are shown at the top of each figure, where $t_\infty = l_\infty/u_\infty$ is the integral time scale. The value of l_∞ was calculated using the relation $l_\infty = 0.1\mathcal{Z}$ and u_∞ was computed using Equation 1, with $\mathcal{Z}$ =13.5 cm. The averaged maximum particle velocity in the (x, y) plane is also shown for each time evolution at the top corner.

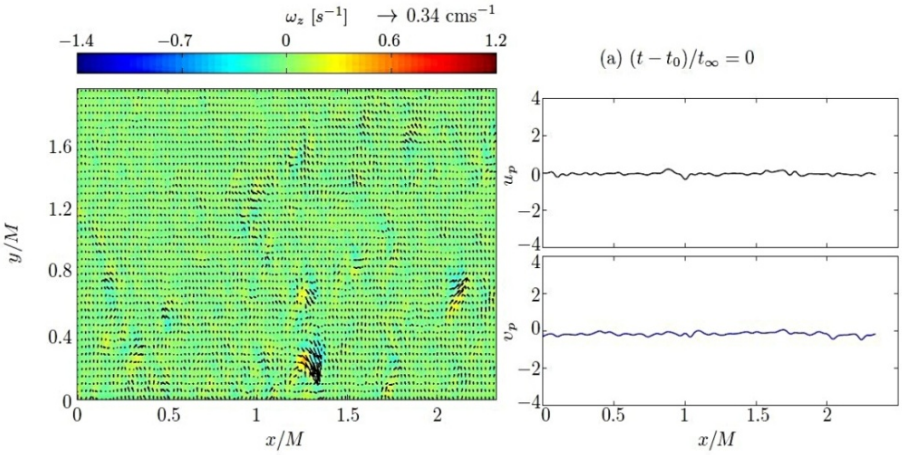

(a)

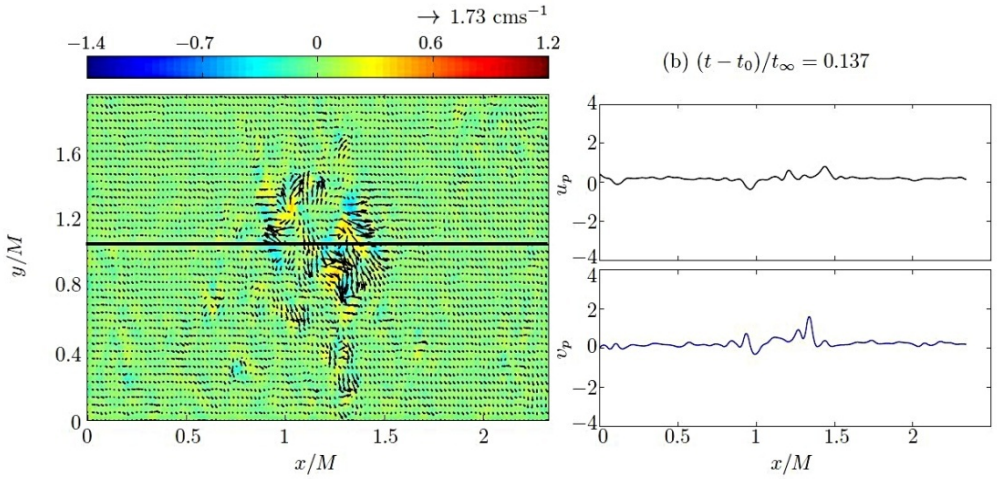
→ 1.73 cms^{-1}
−1.4 −0.7 0 0.6 1.2
(b) $(t-t_0)/t_\infty = 0.137$
y/M
x/M
u_p
v_p

(b)

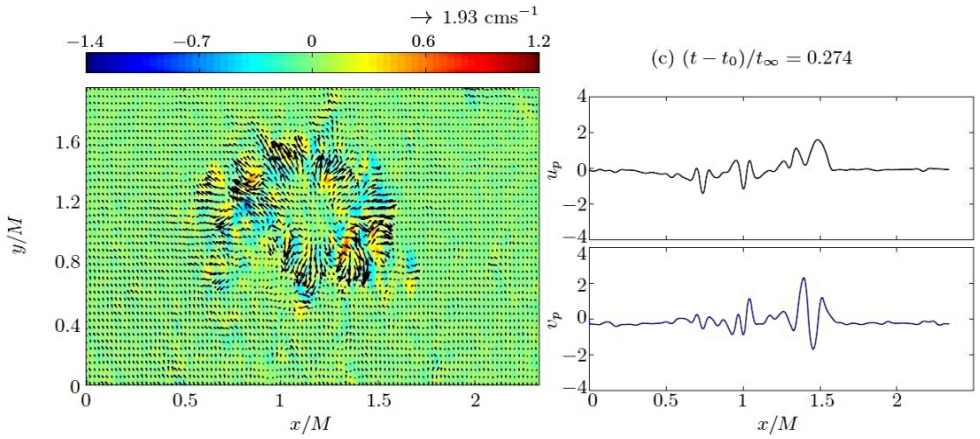
→ 1.93 cms^{-1}
−1.4 −0.7 0 0.6 1.2
(c) $(t-t_0)/t_\infty = 0.274$
y/M
x/M
u_p
v_p

(c)

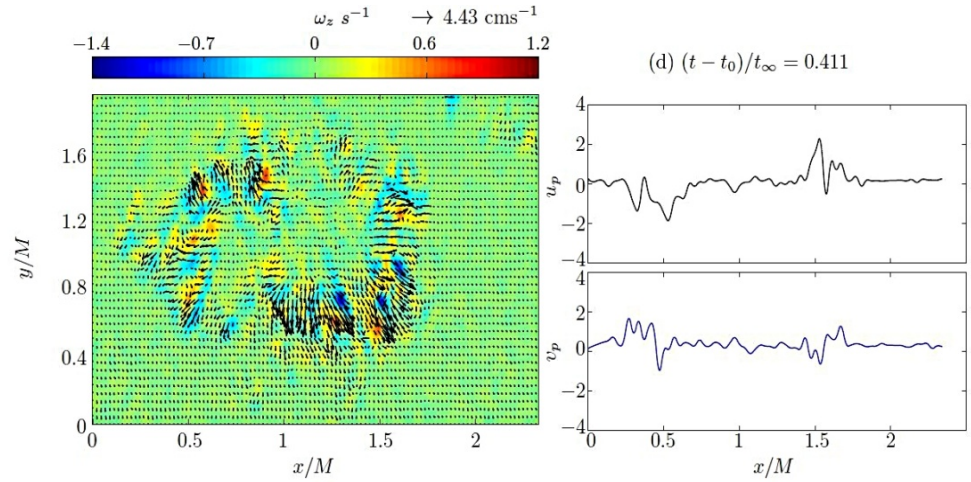
ω_z s^{-1} → 4.43 cms^{-1}
−1.4 −0.7 0 0.6 1.2
(d) $(t-t_0)/t_\infty = 0.411$
y/M
x/M
u_p
v_p

(d)

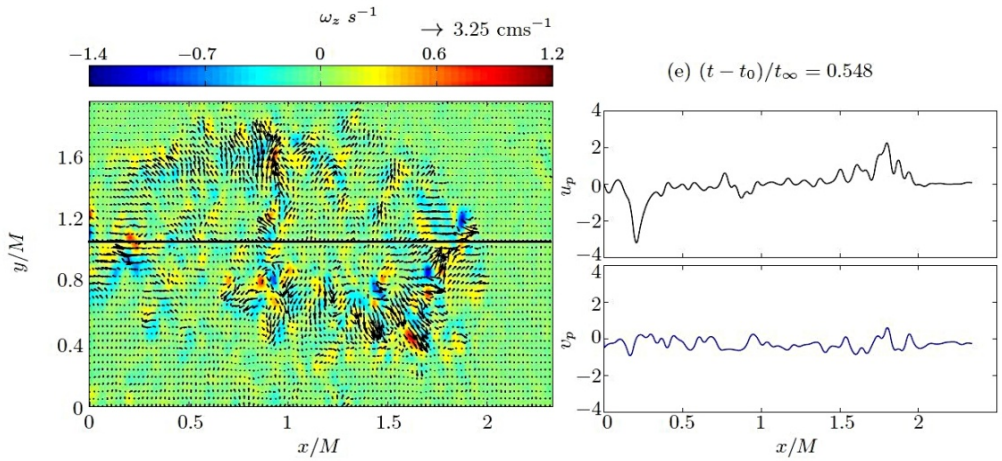
$\omega_z\ s^{-1}$
$\rightarrow 3.25\ \text{cms}^{-1}$
−1.4 −0.7 0 0.6 1.2
(e) $(t-t_0)/t_\infty = 0.548$
y/M
x/M
u_p
v_p

(e)

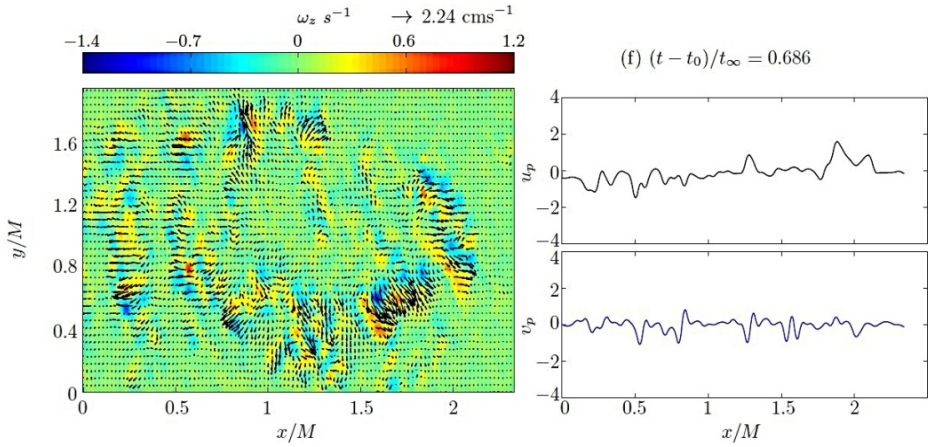
$\omega_z\ s^{-1}$
$\rightarrow 2.24\ \text{cms}^{-1}$
−1.4 −0.7 0 0.6 1.2
(f) $(t-t_0)/t_\infty = 0.686$
y/M
x/M
u_p
v_p

(f)

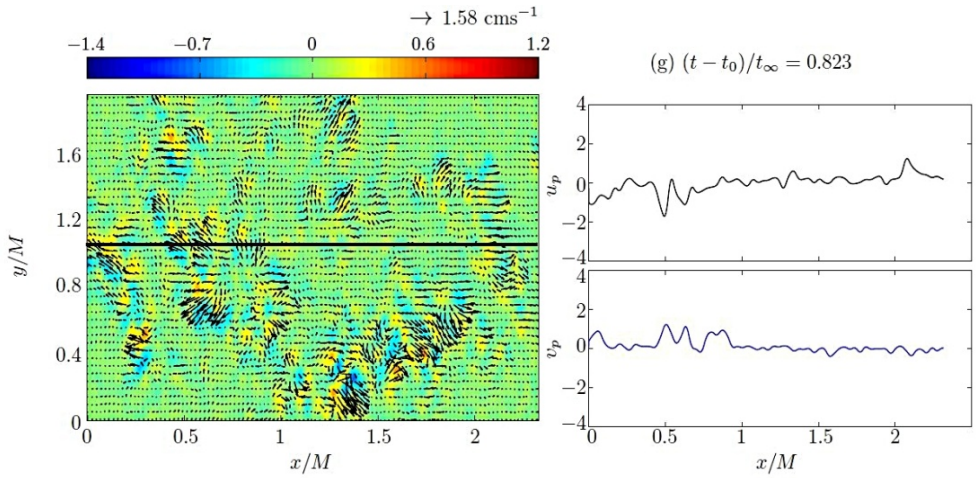
$\rightarrow 1.58\ \text{cms}^{-1}$
−1.4 −0.7 0 0.6 1.2
(g) $(t-t_0)/t_\infty = 0.823$
y/M
x/M
u_p
v_p

(g)

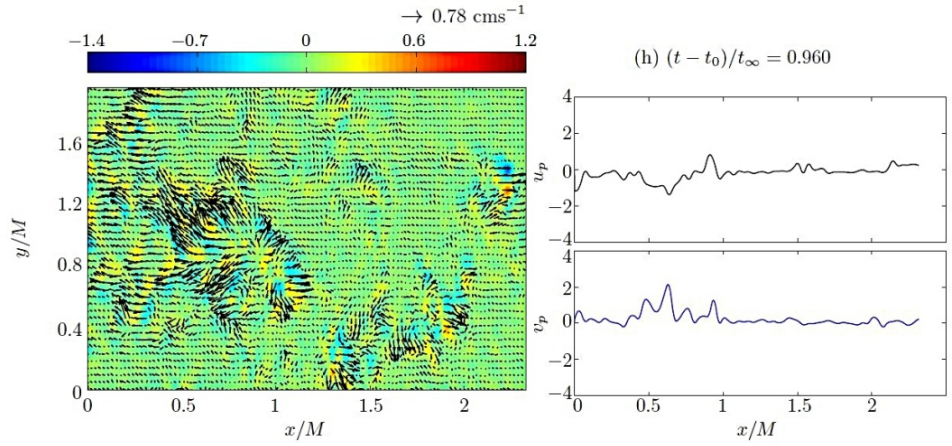

(h)

Fig. 4: Sequences of measured particle velocity fields for Particle B d = 751μm) with vorticity $\omega_z = \partial u_p/\partial y - \partial v_p/\partial x$ distributions (shown as left figure) and corresponding horizontal u_p and transverse particle velocity v_p at a fixed point obtained at corresponding dimensionless times with t_∞ = 1.525. The impact shown corresponds to turbulence produced from S = 8 cm, f = 3 Hz, θ/θ_c = 4.76 interacting with a sediment layer of particle H. Correspond maximum horizontal particle velocity is shown on the top right corner of left figure. The solid black line in (b) illustrates the corresponding y −point where u_p and v_p were taken.

Figure 3a to e and 4a to h illustrate that the typical particle trajectories take the form of a circular splash with dominant horizontal and transverse particle velocities. At other regions where, $\theta < \theta_c$, no trajectory was observed. As an energetic eddy approaches the bed surface, momentum is transferred from the fluid vertical velocity component to the motion parallel to the bed surface (i.e., horizontal and transverse fluid velocity) due to the formation of a splat event (Perot and Moin, 1995). The increasing momentum in the transverse plane induces bed shear stress in the near-bed region. During interaction, the bed shear stress increases and acts to thin the inner viscous sub layer, thereby exposing the near-surface sediment grains in this region to greater hydrodynamic drag and lift forces (Munro *et al*., 2009). At $(t - t_0)/t_\infty = 0$, significant particle movement was not detectable. When the condition $\theta < \theta_c$ is satisfied, near surface sediment grains are brought into motion. At this point in time, the sediment grains are subjected to a nonzero component of horizontal and transverse fluid velocity which acts to propel them away from the bed surface, forming the characteristic particle splash. Consequently, the PIV started to capture the particle movement, giving a corresponding increase to u_p and v_p (in two opposite directions). For example, Fig. 3b shows two distinct peaks of u_p and v_p (at $t = 0.104t_\infty$). Note that u_p and v_p increased within the same distance *x/M* (Fig. 3). Corresponding increasing particle velocities u_p and v_p suggesting that the particles movement is induced by the splat events. Detailed discussion on splat events is referred to the work of Perot and Moin (1995) and Bodart *et al*. (2010). As the stretched eddy diameter increases, the radius of splash increases. Both u_p and v_p also increase until reaching an instantaneous peak velocity at $t = 0.21t_\infty$ and $t = 0.21\ t_\infty$ for Particle A and B, respectively, where at this point the bed shear stress is maximum. Note that at this point ($t = 0.21\ t_\infty$) in Fig. 3, the length of intense particle motion with high u_p and v_p is approximately $1M$. In Fig. 4 for Particle B, however where u_p reached peak velocity at $t = 0.41t_\infty$, the length of visible particle movement is approximately $1.3\,M$. For both particle types, the integral length scale within the homogeneous region l_∞ is approximately 1.4 cm. Thus, the maximum length (i.e., at peak velocity) of sediment movement induced by the energetic eddy (in terms of l_∞ is 3.57 and 4.64 for Particle A and Particle B, respectively. After the peak velocity is reached, the bed shear stress starts to decay. Even so, they are still high to induce particle movement and the radius of splash still increasing. Subsequently, horizontal and transverse particle velocities u_p and v_p, respectively start to decrease and the length where the particle motion were seen, are to be decreasing too. Decreasing shear stress resulted in fewer entrained particles and insufficient energy to keep the particle in motion. When the bed shear stress is no longer sufficient to induce particle movement,

particles were settled back to the bed. At this point, the PIV detected no significant particle movement and the circular splash disappeared. Note that for Fig. 4h at $\frac{(t-t_0)}{t_\infty} = 0.96$, the intense particle motion between $0.5 \leq x/M \leq 1$ is a new energetic interaction.

For the data set used in Fig. 3 and 4, although a circular sediment displacement was observed, over the splash period of interaction, the particle trajectories were seen not to be able to sustain a coherent circular displacement (Fig. 3d and 4d). The reason behind this could be the fact that the horizontal and transverse fluid velocities acting on the particles (in the isolated spots) have been dissipated by the viscous forces. Viscous friction along the bed prevents the total amount of kinetic energy being transferred to the tangential components (by splat events) (Hunt and Graham, 1978; Perot and Moin, 1995; Bodart *et al*., 2010). Thus, the fluid velocities (in the transverse plane) acting on the particles are reduced and the energy available is not sufficient to keep the particles in (intense) motion. Another possible reason is due to the low intensity of the particle movement, whereby the movement of particles was not able to be picked up by PIV.

Both examples show that the duration of particle movement induced by energetic eddies is within one eddy turnover time (equivalent to t_∞), in the figures shown $t = 0.52t_\infty$ and $t = 0.96t_\infty$ for Particle A and B, respectively. Note that although θ/θ_c are comparable between the two cases discussed, the maximum diameter of circular splash attained for Particle B (Fig. 4) is approximately $2M$, where as for Particle A (Fig. 3), the maximum diameter is approximately $1.1M$. The longer sediment displacement and larger splash diameter for Particle B is because the particles are easily entrained into the turbulence structure above the bed due to its low particle relaxation time (i.e. low density). It was also observed that the mode of sediment grain displacement for particle B was dominantly rolling. Rolling particles moved with a persistent contact with bed resulted energy (transferred from the high momentum fluid) within the particles has always need to overcome the resistance forces (imposed by the bed), leading to more energy dissipation. As the bed is mobile, the effective friction coefficient is higher, enhancing the momentum transfer to the bed (Lajeunesse *et al*., 2010). Thus, the energy within the level of flow strength discussed (for Particle A) to induce particle motion, is reduced. Particle B, however was observed to move dominantly in a saltating mode. Saltating particles are entrained into the outer flow, have minimum contact with sediment bed and are easily entrained by the turbulence structure. This gives longer times and distances of particle displacement for Particle B. Under the turbulence-particle interaction discussed here, the distance of particle displacements induced by the turbulence are found up to approximately $41.2d$ and approximately $91.2d$ away from the eddy centre for Particle A and B, respectively. Recall that d is the sediment size.

It is worth highlighting that as the fluid velocity in the near-bed region was not spatially measured, the spatial fluid velocity `i.e.' instantaneous horizontal and vertical fluid velocities evolution along the bed surface could not be investigated. Thus, a detailed analysis on how the splat and antis plat events interact and move sediment is currently not feasible.

CONCLUSION

The experiments described here examined the particle trajectories induced by a zero-mean oscillating-grid generated turbulence. Two sediment types were used with comparable $d \approx 700$ μm and the fluid strength is $\frac{\theta}{\theta_c} \gg 1$. The adaptation of using PIV to measure particle velocities was able to identify circular (splash) particle trajectories. The circular mound of displaced sediment grains indicates that the particles are primarily displaced by radial (tangential) velocities. This is supported by the increasing horizontal u_p and transversal v_p particle velocities during the period of interaction, where horizontal and transverse particle velocities increased as the energetic eddy approached and stretched along the bed surface, attaining peak values at $\frac{(t-t_0)}{t_\infty} \approx 0.41$ for Particle B and $\frac{(t-t_0)}{t_\infty} \approx 0.25$ for Particle type A, respectively. After reaching peak values, both u_p and v_p decrease to zero as the bed shear stress decays. Consequently, the turbulence is no longer sufficient to maintain sediment movement and the circular splash is disappeared. These preliminary experiments provide an initial setup for future work on employing the zero-mean turbulence and to study its interaction with a sediment layer. Further experiments to investigate the particle behaviour under higher $\frac{\theta}{\theta_c} \gg 1$ and varying sediment type (i.e., density and size) will be beneficial.

REFERENCES

Bellinsky, M., H. Rubin, Y. Agnon, E. Kit and J. Atkinson, 2005. Characteristics of resuspension, settling and diffusion of particulate matter in a water column. Environ. Fluid Mech., 5: 415-441.

Bodart, J., J.B. Cazalbou and L. Joly, 2010. Direct numerical simulation of unsheared turbulence diffusing toward a free-slip or no-slip surface. J. Turbulence, 11: 1-17.

Cheng, N. and A. Law, 2001. Measurements of turbulence generated by oscillating grid. J. Hydraulic Eng., 127: 201-207.

Hopfinger, E.J. and J.A. Toly, 1976. Spatially decaying turbulence and its relation to mixing across density interfaces. J. Fluid Mech., 78: 155-175.

Hunt, J.C.R. and J.M.R. Graham, 1978. Free-stream turbulence near plane boundaries. J. Fluid Mech., 84: 209-235.

Kaftori, D., G. Hetsroni and S. Banerjee, 1995. Particle behavior in the turbulent boundary layer I: Motion, deposition and entrainment. Phys. Fluids, 7: 1095-1106.

Lajeunesse, E., L. Malverti and F. Charru, 2010. Bed load transport in turbulent flow at the grain scale: Experiments and modeling. J. Geophys. Res., 115(F4).

Lamb, M.P., W.E. Dietrich and J.G. Venditti, 2008. Is the critical shields stress for incipient sediment motion dependent on channel-bed slope? J. Geophys. Res., 113(F2).

McLean, S.R., J.M. Nelson and S.R. Wolfe, 1994. Turbulence structure over two-dimensional bed forms: Implications for sediment transport. J. Geophys. Res., 99: 729-747.

Munro, R.J., N. Bethke and S.B. Dalziel, 2009. Sediment resuspension and erosion by vortex rings. Phys. Fluids, 21(4).

Nino, Y. and M.H. Garcia, 1996. Experiments on particle-turbulence interactions in the near-wall region of an open channel flow: Implications for sediment transport. J. Fluid Mech., 326: 285-319.

Perot, B. and P. Moin, 1995. Shear-free turbulent boundary layers. Part 1. Physical insights into near-wall turbulence. J. Fluid Mech., 295: 199-227.

Schmeeckle, M.W., J. Nelson and J. Pitlick, 1998. Direct numerical simulation of bedload sediment transport. Proceedings of the 12th ASCE Engineering Mechanics Conference, La Jolla, May 17-20, CA., USA.

Shields, A., 1936. Application of Similarity Principles and Turbulence Research in Bed-Load Movement. Hydrodynamics Laboratory Publ. No. 167, California Institute of Technology, Pasadena, California, USA.

Sumer, B., L. Chua, N. Cheng and J. Fredsoe, 2003. Influence of turbulence on bed load sediment transport. J. Hydraulic Eng., 129: 585-596.

Valsaraj, K.T., R. Ravikrishna, J.J. Orlins, J.S. Smith, J.S. Gulliver, D.D. Reible and L.J. Thibodeaux, 1997. Sediment-to-air mass transfer of semi volatile contaminants due to sediment resuspension in water. Adv. Envirov. Res., 1: 145-156.

Wu, B., D.S. Van Maren and L. Li, 2008. Predictability of sediment transport in the yellow river using selected transport formula. Int. J. Sed. Res., 23: 283-298.